An, Y., Li, S.M., Zhu, D.C., Cawood, P.A., Wang, Q., Xie, J.C., Zhang, L.L., and Zhao, Z., 2023, Compositional change from high-Mg to low-Mg magmatism at ca. 150 Ma in the central Lhasa terrane, Tibet: Switching from advancing to retreating subduction of the Bangong Tethys slab: GSA Bulletin, https://doi.org/10.1130/B36719.1.

Supplemental Material

Supplemental Text S1. Analytical Methods.

Table S1. LA-ICP-MS zircon trace element results for intrusive rocks from the Zhegu, Wengmunong, and Dulu plutons in the central Lhasa subterrane.

Table S2. LA-ICP-MS zircon U-Pb dating results for intrusive rocks from the Zhegu, Wengmunong, and Dulu plutons in the central Lhasa subterrane.

Table S3. In-situ zircon Hf isotopes analyzed by LA-MC-ICP-MS for intrusive rocks from the Zhegu, Wengmunong, and Dulu plutons in the central Lhasa subterrane.

Table S4. Whole-rock major and trace element concentrations for intrusive rocks from the Zhegu, Wengmunong, and Dulu plutons in the central Lhasa subterrane, and for duplicate samples and measured USGS standards.

Table S5. Compiled GPS positions and zircon U-Pb age data of the magmatic rocks from the central and southern Lhasa subterranes.

Table S6. Compiled GPS positions and detrital zircon U-Pb age and Hf isotopic data of sedimentary rocks from Mesozoic strata in the central and southern Lhasa subterranes.

Figure S1. Whole-rock TiO_2, Al_2O_3, TFe_2O_3, MgO, CaO, and Na_2O versus SiO_2 diagrams (A–F) for intrusive rocks from the Zhegu, Wengmunong, and Dulu plutons in the central Lhasa subterrane.

Figure S2. (A) Whole-rock $\varepsilon Nd(t)$ and (B) whole-rock $(^{87}Sr/^{86}Sr)_i$ versus zircon U-Pb age diagrams for Middle Jurassic-Early Cretaceous igneous rocks in the central Lhasa subterrane.

Figure S3. Ba/Th versus La/Sm (A) and Zr and Ba versus SiO_2 (B–C) diagrams for Middle-Late Jurassic igneous rocks in the central Lhasa subterrane.

Yu An, Shi-Min Li*, Di-Cheng Zhu*, Peter A. Cawood, Qing Wang, Jin-Cheng Xie, Liang-Liang Zhang, and Zhidan Zhao, 2022, Compositional change from high-Mg to low-Mg magmatism at ca. 150 Ma in central Lhasa Terrane, Tibet: switching from advancing to retreating subduction of the Bangong Tethys: GSA Bulletin.

Supplemental Material

1. ANALYTICAL METHODS

1.1. Zircon trace elemental analyses and U-Pb dating

1.2. In-situ zircon Hf isotope measurements

1.3. Whole-rock geochemical analyses

2. DATA SETS AND FIGURES

Table S1. LA-ICP-MS zircon trace element results for intrusive rocks from the Zhegu, Wengmunong, and Dulu plutons in the central Lhasa subterrane.

Table S2. LA-ICP-MS zircon U-Pb dating results for intrusive rocks from the Zhegu, Wengmunong, and Dulu plutons in the central Lhasa subterrane.

Table S3. In-situ zircon Hf isotopes analyzed by LA-MC-ICP-MS for intrusive rocks from the Zhegu, Wengmunong, and Dulu plutons in the central Lhasa subterrane.

Table S4. Whole-rock major and trace element concentrations for intrusive rocks from the Zhegu, Wengmunong, and Dulu plutons in the central Lhasa subterrane, and for duplicate samples and measured USGS standards.

Table S5. Compiled GPS positions and zircon U-Pb age data of the magmatic rocks from the central and southern Lhasa subterranes.

Table S6. Compiled GPS positions and detrital zircon U-Pb age and Hf isotopic data of sedimentary rocks from Mesozoic strata in the central and southern Lhasa subterranes.

Figure S1. Whole-rock TiO_2, Al_2O_3, TFe_2O_3, MgO, CaO, and Na_2O versus SiO_2 diagrams (A–F) for intrusive rocks from the Zhegu, Wengmunong, and Dulu plutons in the central Lhasa subterrane.

Figure S2. (A) Whole-rock $\varepsilon_{Nd}(t)$ and (B) whole-rock $(^{87}Sr/^{86}Sr)_i$ versus zircon U-Pb age diagrams for Middle Jurassic-Early Cretaceous igneous rocks in the central Lhasa subterrane.

Figure S3. Ba/Th versus La/Sm (A) and Zr and Ba versus SiO_2 (B–C) diagrams for Middle-Late Jurassic igneous rocks in the central Lhasa subterrane.

3. REFERENCE CITED

1. ANALYTICAL METHODS

1.1. Zircon trace elemental analyses and U-Pb dating

Eight samples were selected for zircon U-Pb dating. U-Th-Pb isotopes and trace elements of zircons were analyzed synchronously using an Agilent 7900 ICP-MS system combined with a NewWave 193^{UC} excimer laser ablation (LA) system at the Milma Lab, China University of Geosciences, Beijing (CUGB). The laser denudation diameter of 35 um, the repetition rate of 6–8 Hz, and the energy density of 4–6 J/cm^2 were used for all spot analyses. Each spot analysis consisted of background acquisition of 18 s (gas blank), sample integration of 50 s, and a delay of 30 s to washout and prepare for the next spot analysis. We use zircon 91,500 (Wiedenbeck et al., 1995) and glass NIST SRM 610 as external standards to correct U-Pb age and trace elements, respectively. Zircon GJ-1 (Jackson et al., 2004) and Plešovice (Sláma et al., 2008) were used as monitor standards to examine the instrument state and the accuracy of the calibration. Detailed setting parameters and conditions for the LA system and ICP-MS equipment are consistent with the introductions in Zhang et al. (2019). The ICPMSDataCal (Liu et al., 2010), a Microsoft software, was applied to conduct off-line analyses of data. The common Pb correction, concordia diagram plotting, and weighted mean age calculation were carried out by using the ComPbCorr#3.17 (Andersen, 2002) and ISOPLOT (ver 3.0) (Ludwig, 2003), respectively. The concordance degree was calculated by the ratio of $^{207}Pb/^{235}U$ and $^{208}Pb/^{238}U$ ages and data with discordance larger than 10% were eliminated. Uncertainties for individual analyses are reported at 1-sigma and mean $^{206}Pb/^{238}U$ analyses at 2-sigma.

1.2. In-situ zircon Hf isotope measurements

Zircon in-situ Hf isotopes were analyzed on the same zircon grains previously analyzed for U-Pb dating at Milma Lab, CUGB by using multi-collector (MC)-ICP-MS attached to a New Wave 193^{UC} excimer LA system. During analysis, the spot size of 35 μm, the laser repetition rate of 6 Hz, and the energy density of 3–4 J/cm^2 were applied for all spot analyses. Each analysis includes background acquisition of 50 s, data acquisition of 50 s, and washout of 5 s. The detailed setting parameters and analytical procedures were described by Zhang et al. (2019). Zircon 91500 (Blichert-Toft, 2008) was analyzed as the external standard for correcting mass discrimination, and zircon standards GJ-1(Jackson et al., 2004) and Plesovice (Sláma et al., 2008) were used as unknown samples. Raw data were processed by using Iolite software (Paton et al., 2011). We calculate zircon $\varepsilon_{Hf}(t)$ values reported in this study and literature using the Chondrite Lu-Hf isotopic values ($^{176}Lu/^{177}Hf$ = 0.0336 and $^{176}Hf/^{177}Hf$ = 0.282785; Bouvier et al., 2008).

1.3. Whole-rock geochemical analysis

Twenty-five samples were analyzed for major and trace element compositions. Whole-rock major element oxides (wt.%) were measured on fused glass discs, using X-ray fluorescence (Axios MAX) at Chinese Academy of Sciences, Beijing, China. The analytical uncertainties are generally better than 5% for all elements. Whole-rock trace elements were measured using Agilent 7700e ICP-MS at the Wuhan SampleSolution Analytical Technology Co., Ltd., Wuhan, China. Multiple-reference materials, including AGV-2, BHVO-2, BCR-2, and RGM-2, were used to calibrate the elemental concentrations of samples. The accuracy is commonly better than 10%.

2. DATA SETS AND FIGURES

Tables S1–S6 are listed in an Excel file

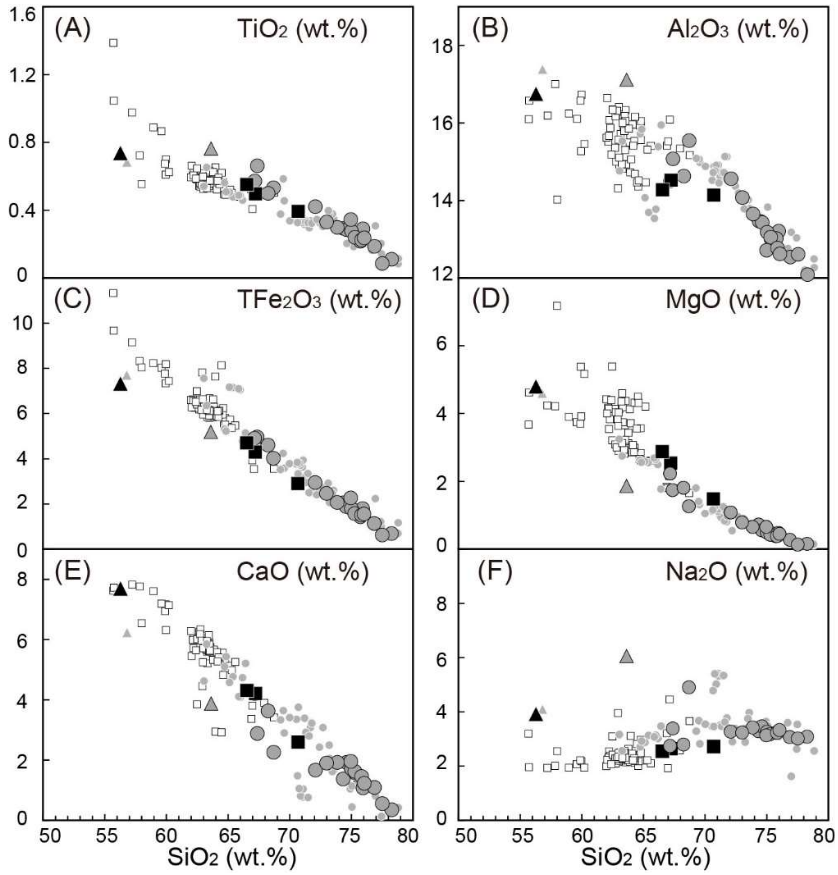

Figure S1. (A–F) Whole-rock TiO_2, Al_2O_3, TFe_2O_3, MgO, CaO, and Na_2O versus SiO_2 diagrams for intrusive rocks from the Zhegu, Wengmunong, and Dulu plutons in the central Lhasa subterrane. The sources of literature data are the same as in Figure 5.

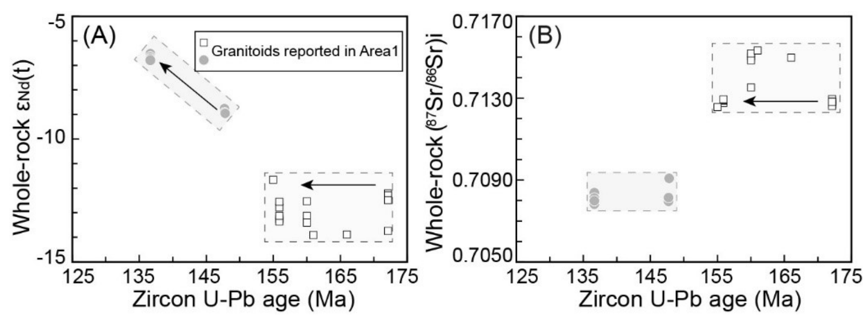

Figure S2. (A) Whole-rock $\varepsilon_{Nd}(t)$ and (B) whole-rock $(^{87}Sr/^{86}Sr)_i$ values versus zircon U-Pb ages diagrams for Middle Jurassic-Early Cretaceous igneous rocks in the central Lhasa subterrane. Literature data are from Wang et al. (2017), Liu et al. (2018), Zheng et al. (2018), Wu et al. (2021), and Tong et al. (2022).

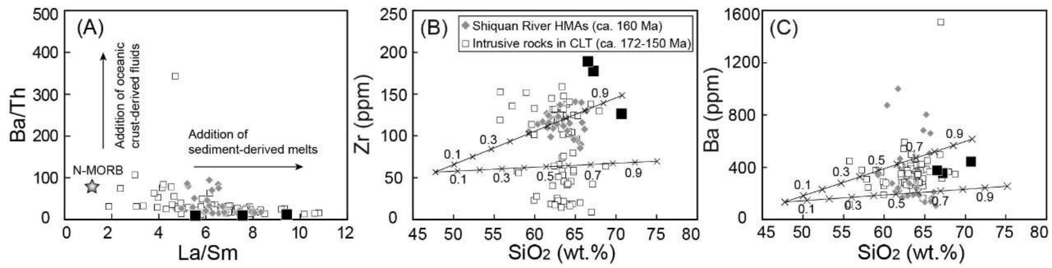

Figure S3. Ba/Th versus La/Sm (A) and Zr and Ba versus SiO_2 (B–C) diagrams for Middle-Late Jurassic igneous rocks in the central Lhasa subterrane. MORB = mid ocean ridge basalt. N-MORB = normal MORB. The data for N-MORB and Shiquan River high-Mg andesites (HMAs) are from Gale et al. (2013) and Liu et al. (2018), respectively. Data sources of intrusive rocks (172–150 Ma) are listed in Table S5.

3. REFERENCE CITED

Andersen, T., 2002, Correction of common lead in U-Pb analyses that do not report ^{204}Pb: Chemical Geology, v. 192, p. 59–79, https://doi.org/10.1016/s0009-2541(02)00195-x.

Blichert-Toft, J., 2008, The Hf isotopic composition of zircon reference material 91500: Chemical Geology, v. 253, p. 252–257, https://doi.org/10.1016/j.chemgeo.2008.05.014.

Bouvier, A., Vervoort, J.D., and Patchett, P.J., 2008, The Lu-Hf and Sm-Nd isotopic composition of CHUR: Constraints from unequilibrated chondrites and implications for the bulk composition of terrestrial planets: Earth and Planetary Science Letters, v. 273, p. 48–57, https://doi.org/10.1016/j.epsl.2008.06.010.

Gale, A., Dalton, C.A., Langmuir, C.H., Su, Y., and Schilling, J.-G., 2013, The mean composition of ocean ridge basalts: Geochemistry, Geophysics, Geosystems, v. 14, p. 489–518, https://doi.org/10.1029/2012gc004334.

Jackson, S.E., Pearson, N.J., Griffin, W.L., and Belousova, E.A., 2004, The application of laser ablation-inductively coupled plasma-mass spectrometry to in situ U–Pb zircon geochronology: Chemical Geology, v. 211, p. 47–69, https://doi.org/10.1016/j.chemgeo.2004.06.017.

Liu, W.-L., Huang, Q.-T., Gu, M., Zhong, Y., Zhou, R., Gu, X.-D., Zheng, H., Liu, J.-N., Lu, X.-X., and Xia, B., 2018, Origin and tectonic implications of the Shiquanhe high-Mg andesite, western Bangong suture, Tibet: Gondwana Research, v. 60, p. 1–14, https://doi.org/10.1016/j.gr.2018.03.017.

Liu, Y., Gao, S., Hu, Z., Gao, C., Zong, K., and Wang, D., 2010, Continental and Oceanic Crust Recycling-induced Melt-Peridotite Interactions in the Trans-North China Orogen: U-Pb Dating, Hf Isotopes and Trace Elements in Zircons from Mantle Xenoliths: Journal of Petrology, v. 51, p. 537–571, https://doi.org/10.1093/petrology/egp082.

Ludwig, K.R., 2003, ISOPLOT 3.00: A geochronological toolkit for Microsoft Excel, Berkeley, CA, Berkeley Geochronology Center.

Paton, C., Hellstrom, J., Paul, B., Woodhead, J., and Hergt, J., 2011, Iolite: Freeware for the visualisation and processing of mass spectrometric data: Journal of Analytical Atomic Spectrometry, v. 26, p. 2508–2518, https://doi.org/10.1039/c1ja10172b.

Sláma, J., Košler, J., Condon, D.J., Crowley, J.L., Gerdes, A., Hanchar, J.M., Horstwood, M.S.A., Morris, G.A., Nasdala, L., Norberg, N., Schaltegger, U., Schoene, B., Tubrett, M.N., and Whitehouse, M.J., 2008, Plešovice zircon — A new natural reference material for U-Pb and Hf isotopic microanalysis: Chemical Geology, v. 249, p. 1–35, https://doi.org/10.1016/j.chemgeo.2007.11.005.

Tong, X., Yan, J., Zhao, Z., Niu, Y., Qi, N., Shi, Q., Liu, D., Wang, Q., Zhang, L.-L., Dong, G., and Zhu, D.-C., 2022, Middle-Late Jurassic magmatism in the west central Lhasa subterrane, Tibet: Petrology, zircon chronology, elemental and Sr-Nd-Pb-Hf-Mg isotopic geochemistry: Lithos, v. 408–409, no. 106549, https://doi.org/10.1016/j.lithos.2021.106549.

Wang, Y., Tang, J., Wang, L., Duan, J., Danzhen, W., Li, S., and Li, Z., 2017, Petrogenesis of Jurassic granitoids in the west central Lhasa subterrane, Tibet, China: the Geji example: International Geology Review, v. 60, p. 1155–1171, https://doi.org/10.1080/00206814.2017.1375438.

Wiedenbeck, M., Allé, P., Corfu, F., Griffin, W.L., Meier, M., Oberli, F., Von Quadt, A., Roddick, J.C. Spiegel, W., 1995, Three natural zircon standards for U-Th-Pb, Lu-Hf, trace element and REE analyses: Geostandards and Geoanalytical Research, v. 19, p. 1–23, https://doi.org/10.1111/j.1751-908X.1995.tb00147.x.

Wu, H., Fan, J.-J., Jiang, Z.-Q., Hao, Y.-J., and Luo, A.-B., 2021, Late Jurassic-Early Cretaceous magmatic activity in the Central Lhasa Terrane: Petrogenesis and implications for the initial subduction of the Slainajap oceanic lithosphere: Palaeogeography, Palaeoclimatology, Palaeoecology, v. 573, no. 110438, https://doi.org/10.1016/j.palaeo.2021.110438.

Zhang, L.-L., Zhu, D.-C., Wang, Q., Zhao, Z.-D., Liu, D., and Xie, J.-C., 2019, Late Cretaceous volcanic rocks in the Sangri area, southern Lhasa Terrane, Tibet: Evidence for oceanic ridge subduction: Lithos, v. 326–327, p. 144–157, https://doi.org/10.1016/j.lithos.2018.12.023.

Zheng, H., Huang, Q.T., Cai, Z.R., Zhang, K.J., Liu, H.C., Cheng, C., Lu, L.J., Yang, P., Yu, S.R., and Yang, G., 2018, Early Cretaceous arc granitoids from the central Lhasa subterrane: Production of the northward subduction of Yarlung Zangbo Neo-Tethyan Ocean?: Geological Journal, v. 54, p. 4001–4013, https://doi.org/10.1002/gj.3399.